2022 IEEE Applied Power Electronics Conference and Exposition (APEC)
Houston, TX, USA

Core Size Scaling Law of Two-Phase Coupled Inductors – Demonstration in a 48-to-1.8 V Hybrid Switched-Capacitor MLB-PoL Converter

T. Ge
R. A. Abramson
Z. Ye
R. C. N. Pilawa-Podgurski

Core Size Scaling Law of Two-Phase Coupled Inductors – Demonstration in a 48-to-1.8 V Hybrid Switched-Capacitor MLB-PoL Converter

Ting Ge, Rose Abramson, Zichao Ye, and Robert C.N. Pilawa-Podgurski
Department of Electrical Engineering and Computer Sciences
University of California, Berkeley
Email: {gting, rose_abramson, yezichao, pilawa}@berkeley.edu

***Abstract*—Conventional design of coupled inductors is focused on a specific converter topology, and the size advantage of coupled inductors over uncoupled inductors is rarely analyzed systematically. This work models the core size for generalized two-phase gapped coupled inductors and provides an effective way to compare the core size for different duty ratios (corresponding to different topologies) and different coupling coefficients. Both the analytical model and hardware prototypes are provided to demonstrate a significant size reduction by using tightly-coupled inductors in hybrid switched-capacitor converters with a large duty ratio. The proposed coupled inductors are applied in a Multi-Level Binary (MLB) Point-of-Load (PoL) converter, achieving 94.4% peak system efficiency and 474 W/in^3 power density with 48-to-1.8 V conversion and 60 A output. Both the efficiency and power density are higher than the conventional MLB-PoL converter using discrete inductors.**

***Keywords*—coupled inductors, core size scaling, hybrid SC converter**

I. Introduction

Due to their small size, low loss, and fast transient response, coupled inductors have been widely used in dc-dc power converters [1]–[3]. A distinct feature of coupled inductors is the current ripple cancelling effect, which helps reduce winding loss and the required inductance [4], [5]. Although much research work has qualitatively demonstrated that coupled inductors can achieve smaller core size, it is rarely reported by what percentage the core size can be reduced using different coupling coefficients. In this work, a magnetic-flux-based core size scaling law is presented to quantify the relationship between the required core size and the coupling coefficient to guide magnetic design. Furthermore, the model can be extended to various converter topologies, in which the inductor sees different duty ratios.

In Point-of-Load (PoL) applications, coupled inductors are usually employed in multi-phase buck converters, but they are also applicable to emerging hybrid switched-capacitor (SC) converters, such as the series-capacitor buck converter [6], Linear Extendable Group Operated (LEGO) converter [7], and Multi-Level-Binary (MLB) PoL converter [8]. A hybrid SC converter with inductors on the output side can be viewed as a fixed-ratio SC converter cascaded with a multi-phase buck regulator, operated so that the capacitors are soft-charged by the inductors [9], [10]. The SC stage is usually designed to have a high step down ratio, so the buck stage can have a large duty ratio and therefore lower current ripple. This work explores the use of custom coupled inductors in a 48-to-1.8 V MLB-PoL converter. By using a coupling coefficient of -0.75, the resulting core size is 55% smaller than the custom integrated uncoupled inductors and 73% smaller than the commercial discrete inductors. The MLB-PoL converter with coupled inductors achieves 44% higher power density than the best previously published results for the same topology while also having better efficiency.

In this paper, only ferrite gapped inductors are analyzed. Three general modeling assumptions are made to simplify the analysis:

1) Ferrite has infinite permeability, so the air gap rather than the ferrite material stores most of the energy. This means $\mu_r >> l_c/l_g$, where μ_r is the relative permeability of ferrite, l_c is the core length, and l_g is the gap length.

2) The maximum power is limited by the saturation flux density (B_s) and not by inductor loss. This is applicable for PoL converters with hundreds of kHz switching frequency. High-frequency inductors (i.e., MHz or higher) with high core losses are out of the scope of this paper, and not the focus of our model.

3) The ferrite core is fully utilized: all regions of the core are pushed to B_s at the maximum power.

II. Core Size Scaling Law of Coupled Inductors

A. Flux Model of Coupled Inductors

An intuitive way to scale the inductor size is to link the size to energy. A well-known energy equation for a powder-iron inductor is $\frac{1}{2}\int \frac{{B_s}^2}{\mu_r\mu_0} dV_{core} = \frac{1}{2}L{I_{max}}^2$, where V_{core} is the core volume, L is the inductance, and I_{max} is the maximum current through the inductor [11]. The core volume is proportional to ${LI_{max}}^2$. This rule is inaccurate for a ferrite gapped inductor with a core structure as shown in Fig. 1(a), since the energy is stored in the air gap instead of the core. The energy equation is now $\frac{1}{2}\int \frac{{B_s}^2}{\mu_0} dV_{gap} = \frac{1}{2}L{I_{max}}^2$. As shown by the equation, the volume of the air gap $V_{gap} = A_e l_g$ is proportional to ${LI_{max}}^2$. However, now the energy is independent of the core length l_c. The core volume $V_{core} = A_e l_c = \frac{LI_{max} l_c}{NB_s}$ is

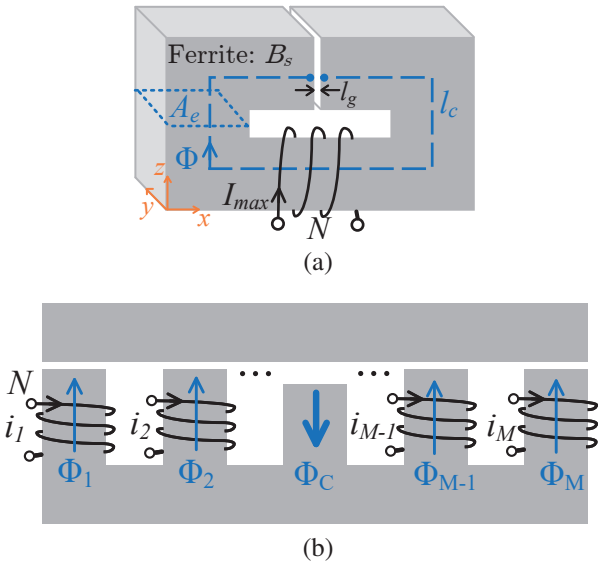

Fig. 1: (a) Single gapped ferrite inductor with core volume proportional to Φ and (b) Coupled inductors with core volume proportional to Φ_{sum}.

proportional to the magnetic flux $\Phi = \frac{LI_{max}}{N}$. It is noted that the core size can be scaled along either the core width (x-axis) or core length (y-axis) direction, as labeled in Fig. 1(a). If the core size is scaled along x-axis, the z-dimension also has to be scaled to maintain a uniform cross-sectional area, and then V_{core} tends to be proportional to Φ^2 not Φ. In this work, we choose y-axis as the direction of core size scaling such that the effective core length l_c is fixed, and the winding window does not impact the linear relationship between V_{core} and Φ.

The size scaling law for a single ferrite inductor then can be extended to multi-winding (M-phase) coupled inductors with the core structure shown in Fig. 1(b). The flux of each side leg is calculated by

$$\begin{bmatrix} \Phi_1 \\ \Phi_2 \\ \vdots \\ \Phi_M \end{bmatrix} = \frac{1}{N} \begin{bmatrix} L_{11} & L_{12} & \cdots & L_{1M} \\ L_{21} & L_{22} & \cdots & L_{2M} \\ \vdots & \vdots & \ddots & \vdots \\ L_{M1} & L_{M2} & \cdots & L_{MM} \end{bmatrix} \begin{bmatrix} i_1 \\ i_2 \\ \vdots \\ i_M \end{bmatrix} \tag{1}$$

where N is the number of turns and is the same for each winding. The flux on the center leg is the sum of the fluxes on side legs, $\Phi_C = \sum_{x=1}^{M} \Phi_x$. The total core volume is proportional to the sum of the maximum flux of each leg, which is given by

$$\Phi_{sum} = \sum_{x=1}^{M} \Phi_{x\_max} + \Phi_{C\_max} \tag{2}$$

Notice that when the windings are operating in interleaving mode, the flux on each leg may not reach the peak simultaneously, and the maximum fluxes Φ_{x_max} (= $max(\Phi_x(t))$) and Φ_{C_max} (= $max(\Phi_C(t))$) should be calculated separately.

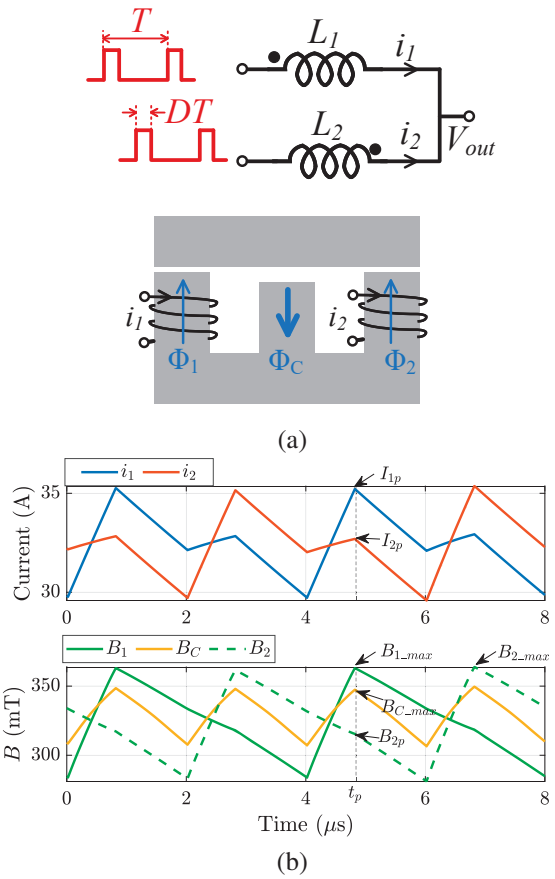

Fig. 2: (a) Schematic, core structure, (b) inductor currents and flux densities of two-phase coupled inductors.

B. Core Size Scaling for Two-Phase Coupled Inductors

This work mainly analyzes the two-phase (M = 2) coupled inductors with the schematic and core structure shown in Fig. 2(a). The corresponding instantaneous flux density on each core leg is shown in Fig. 2(b). According to Eqn. (1) and the waveforms in Fig. 2(b), the side-leg fluxes at time t_p are calculated by:

$$\begin{bmatrix} \Phi_{1\_max} \\ \Phi_{2p} \end{bmatrix} = \begin{bmatrix} L_s & KL_s \\ KL_s & L_s \end{bmatrix} \begin{bmatrix} I_{1p} \\ I_{2p} \end{bmatrix} /N \tag{3}$$

where L_s is the self inductance, and $K(< 0)$ is the coupling coefficient. The currents I_{1p} and I_{2p} are inductor currents at t_p as labeled in Fig. 2(b). The maximum fluxes Φ_{1_max} and Φ_{C_max} are solved from (3)

$$\Phi_{1\_max} = (I_{1p} + KI_{2p})L_s/N = \Phi_{2\_max} \tag{4}$$

$$\Phi_{C\_max} = \Phi_{1\_max} + \Phi_{2p} = (I_{1p} + I_{2p})(1 + K)L_s/N \tag{5}$$

Substituting Eqns. (4) and (5) into (2), we have:

$$\begin{aligned} \Phi_{sum} &= 2\Phi_{1\_max} + \Phi_{C\_max} \\ &= [(3 + K)I_{1p} + (1 + 3K)I_{2p}]L_s/N \end{aligned} \tag{6}$$

Another constraint in the design of coupled inductors is the inductor current ripple, which affects system efficiency and

inductor size. Lower current ripple leads to lower conduction loss and therefore higher efficiency, but requires larger inductance which means larger inductor size. A ripple factor α is defined as the peak-to-peak inductor current over the maximum dc current. For conventional PoL converters, the factor α is usually designed in the range of 0.2 to 0.4 [12]. According to the effective steady-state inductance derived in [2], the self inductance L_s is related to the ripple factor α by

$$L_s = \frac{2V_{out}(1-D+DK)}{f_{sw}I_{out}\alpha(1-K^2)} \tag{7}$$

where f_{sw} is the switching frequency seen by the inductor, and I_{out} is the maximum output current of the converter. The inductor currents are balanced for two phases, so each phase carries a dc current of $\frac{I_{out}}{2}$. By solving for the current ripples in Fig. 2(b), the instantaneous currents I_{1p} and I_{2p} at t_p are calculated by

$$I_{1p} = \frac{I_{out}}{2}(1+\frac{\alpha}{2}) \tag{8}$$

$$I_{2p} = \frac{I_{out}}{2}[1-\frac{\alpha(D+(1-D)K)}{2(1-D+DK)}] \tag{9}$$

Substituting (7), (8), and (9) into equation (6), the total flux is simplified to

$$\Phi_{sum} = \frac{V_{out}}{f_{sw}N}[\frac{4}{\alpha(1-K)} - (\frac{4}{\alpha}+2)D + \frac{3}{2}] \tag{10}$$

Since the total flux Φ_{sum} is proportional to $\frac{V_{out}}{f_{sw}N}$, it can be normalized to

$$\Phi_{sum\_n} = \frac{\Phi_{sum}f_{sw}N}{V_{out}} = \frac{4}{\alpha(1-K)} - (\frac{4}{\alpha}+2)D + \frac{3}{2} \tag{11}$$

As seen from (11), the main factors that affect the total flux or core volume are α, K, and D. The curves of normalized flux Φ_{sum_n} are ploted in Fig. 3(a), showing that increasing $|K|$ and D reduces Φ_{sum_n}, and thus V_{core}. Notice that all the curves are normalized to the same V_{out} and have the same α, which is chosen as 0.3 here.

The duty ratio D is a parameter determined by the converter topology. For the SC-based step-down converter, higher D means a higher step-down ratio of the SC stage and higher duty ratio of the buck-stage inductors. High-D operation is beneficial for not only the inductor size but also the RMS current of the switches, as discussed in [13], [14]. The flux model shown by Eqn. (11) provides a simple way to compare the relative core size between different topologies. For example, at 48-to-1.8 V conversion and α = 0.3, D = 0.0375 for the conventional buck converter and D = 0.3 for the 8-to-1 MLB-PoL converter, leading to $\Phi_{sum\_n@K=0}$ =14.26 and 10.23, respectively. Thus, the D = 0.3 implementation one has 28% smaller core size.

To show by what percentage the core size can be reduced using coupled inductors with different K, each curve in Fig. 3(a) is normalized to 1 at K = 0 and replotted in Fig. 3(b). Core size reduces as $|K|$ increases, and the reduction is more

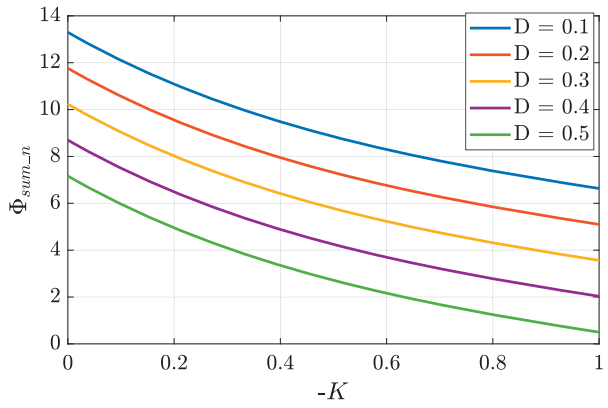

(a)

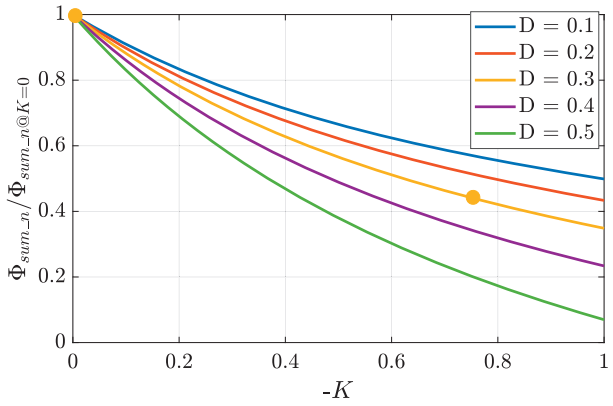

(b)

Fig. 3: (a) Normalized total flux Φ_{sum_n} and (b) the ratio of $\Phi_{sum\_n}/\Phi_{sum\_n@K=0}$ versus $-K$ at α = 0.3.

significant for topologies with higher D. When the converter is operating at $D = 0.5$, the core size needed for highly coupled inductors can be only 1/10 of the uncoupled inductor. Notice that the inductors analyzed in this work are just for PWM converters rather than resonant converters. Although the duty ratio of the gate signal is also 50% for some switched-capacitor resonant converters as introduced in [15], [16], the duty ratio seen by the inductor is extremely small, and the inductor current has a sinusoidal shape. Thus, the core size scaling law of (11) is only applicable for PWM converters.

To better understand the mechanism of coupling-related core size reduction, the total flux Φ_{sum} in (6) can be rewritten as

$$\Phi_{sum} = \underbrace{\frac{\overbrace{(1+K)L_s}^{\text{Leakage L}}(3I_{1p}+I_{2p})}{N}}_{\Phi_{lk}} + \underbrace{\frac{2\overbrace{(-K)L_s}^{\text{Mutual L}}(I_{1p}-I_{2p})}{N}}_{\Phi_M} \tag{12}$$

where Φ_{lk} is the flux induced in the leakage path, and Φ_M is the flux induced in the mutual path. As can be seen from (12), the leakage inductor carries a high current of $3I_{1p}+I_{2p}$, while the mutual inductor carries a low current of $I_{1p}-I_{2p}$ thanks

to a flux-cancelling effect. Therefore, in order to reduce the total core volume, the most effective approach is to reduce the leakage inductance, which can be achieved by increasing the coupling coefficient. According to (7), the required leakage inductance is calculated by $L_{lk} = (1+K)L_s = \frac{2V_{out}(1-D+DK)}{f_{sw}I_{out}\alpha(1-K)}$, showing that L_{lk} decreases as -K increases.

III. Hardware Implementation and Experimental Results

Two points (K = 0, D = 0.3) and (K = -0.75, D = 0.3) as highlighted in Fig. 3(b) are verified experimentally in this section. The converter and inductor specifications are given in Table I. The required self inductance is calculated by (7). The core material is PC95 from TDK, and has a relatively low core loss density at 100 - 300 kHz. The gap length is controlled by polishing the core legs and filling the gap with layers of kapton tape. Specifically, off-the-shelf EI cores PC95EI18/6/10-Z are used to build the coupled and uncoupled inductors with the gap length configuration shown in Fig. 4(b). The major air gap is transferred from the side core legs to the center core leg to realize a high coupling coefficient. After applying the scaling law introduced in Section II, the core length is shortened from 10 mm to 4.5 mm for the coupled inductors. Since both inductors have the same core width and height, the total core size is reduced by 55%.

TABLE I: Converter and inductor specifications

Converter specifications	
V_{in}	48 V
Max. V_{out}	1.8 V
Max. D	0.3
Max. I_{out}	60 A
f_{sw}	250 kHz
α	0.3
Design 1: coupled inductors	
K	-0.75
L_s	800 nH
Design 2: uncoupled inductors	
L	517 nH

Lowering leakage inductance is the main way to achieve small core size. Comparing the uncoupled inductors (K = 0) to coupled inductors ($|K|$ = 0.75), it can be seen that the leakage inductance is reduced by 61%, as shown in Table I, thus reducing core size. Although the leakage inductance is reduced dramatically, the steady-state effective inductance is the same. The measured dc-biased effective inductances for the coupled and uncoupled inductors at $D = 0.3$ are compared in Fig. 5. At zero current, the effective inductance is around 540 nH for both cases. In addition, they have similar saturation currents (defined at 20% inductance drop): 68 A for the uncoupled inductors and 65 A for the coupled inductors.

Both inductors in Fig. 4(b) were then used in a 48-to-1.8 V MLB-PoL converter, which can be viewed as an 8-to-1 SC converter merged with a two-phase interleaved buck converter.

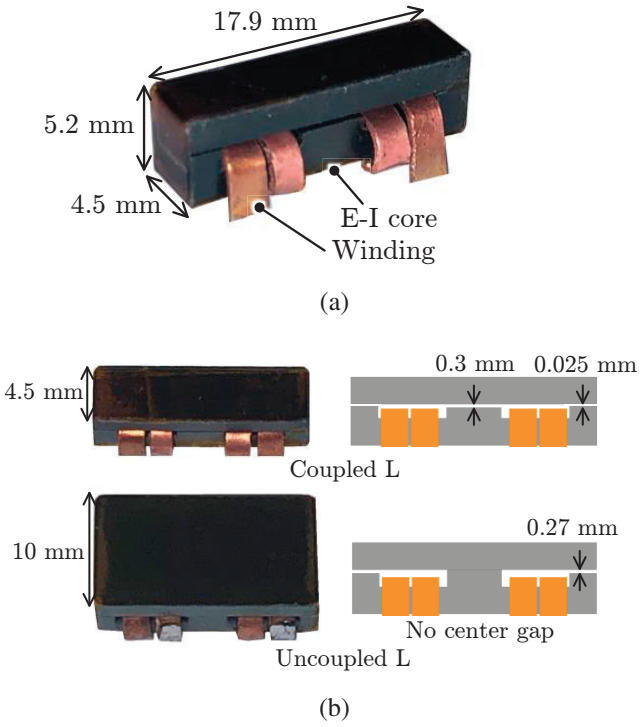

Fig. 4: (a) Annotated photograph of two-phase coupled inductors. (b) Coupled inductors have 55% smaller length than the uncoupled inductors. They have the same core width and height.

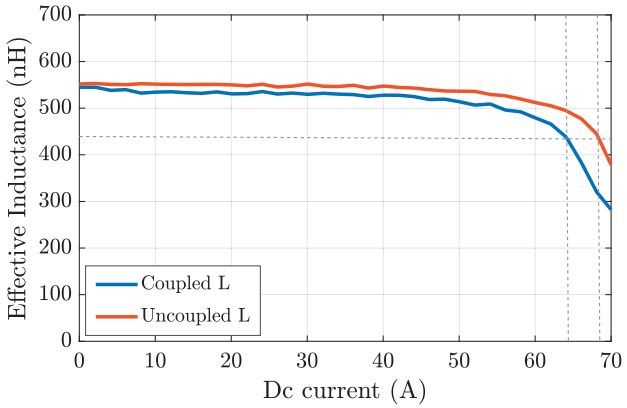

Fig. 5: Measured steady-state effective inductances for coupled and uncoupled inductors in Fig. 4(b) with $D = 0.3$ and f_{sw} = 250 kHz, demonstrating that they have similar effective inductance and saturation current.

This converter features multi-phase operation that can help achieve high conversion ratio with a low component count. The output inductors in this converter benefit from a frequency multiplication effect, i.e., the frequency seen by the inductors is higher than the switching frequency. This effect helps reduce the inductor size without increasing the switching frequency. The detailed operation principle of the MLB-PoL converter is introduced in [8]. The annotated picture of the hardware

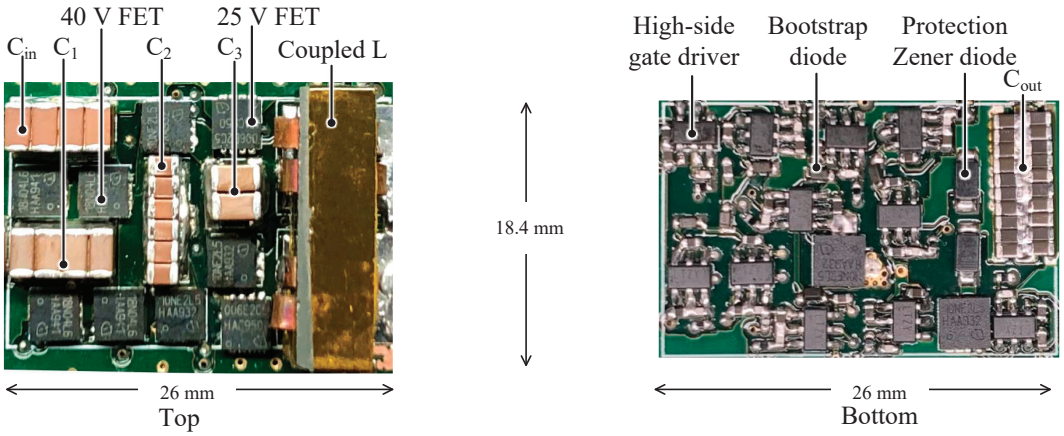

Fig. 6: Annotated photograph of MLB-PoL converter with the dimensions of 26 × 18.4 × 7.8 mm (1.02 × 0.72 × 0.31 inch).

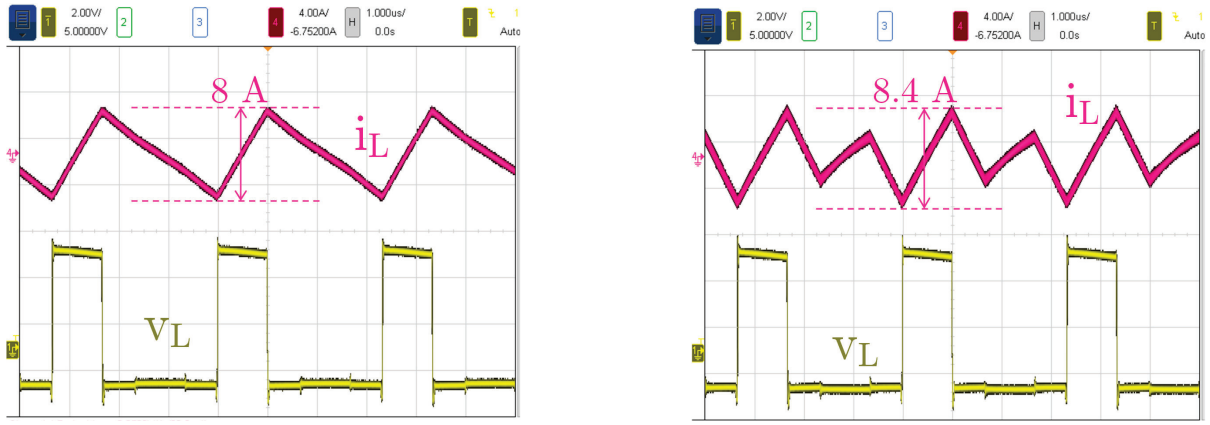

(a) (b)

Fig. 7: Measured inductor current ripple (ac coupled) for (a) uncoupled inductors and (b) coupled inductors at I_{out} = 30 A, demonstrating that they have similar effective inductances.

prototype is shown in Fig. 6. All main components are tightly placed in a rectangular box with a footprint of 26 × 18.4 mm. The total height of this converter is 7.8 mm including the PCB thickness and the components on both sides. If the coupled inductors are replaced by the uncoupled inductors in Fig. 4(b), the footprint of the top-side components would increase to 31.5 × 18.4 mm.

The measured inductor current waveforms with and without magnetic coupling are shown in Fig. 7. The current ripple is ∼8 A for both cases, which satisfies the design target ($\alpha I_{out\_max}/2$ = 9 A) in Table I. In summary, the coupled and uncoupled inductors have similar steady-stage effective inductance, current ripple, and saturation current, while the core size of the coupled inductors is reduced by half. Another advantage of the coupled inductors is the lower transient inductance, which means a faster transient response. A detailed analysis of transient performance of the coupled inductors is introduced in [2].

The measured efficiencies including gate drive loss are shown in Fig. 8. Both inductors have similar efficiencies since they have similar current ripple and similar conduction loss for the switches. The switching loss is also similar for the two cases since they have the same voltage stress and turn-on/off current. The converter using uncoupled inductors has a slightly higher peak efficiency because it has lower harmonic currents and lower core loss. At heavy load, the coupled inductors achieve slightly higher efficiency as they have lower winding resistance.

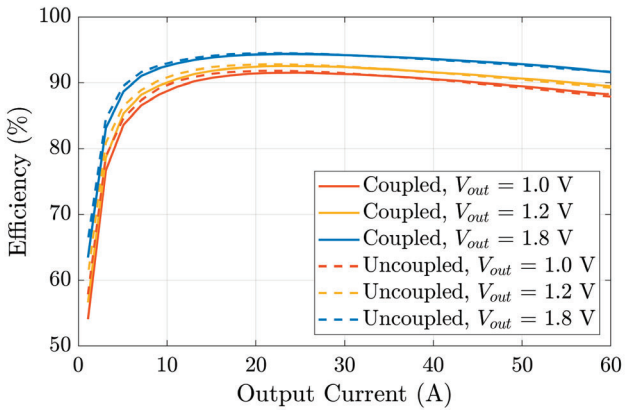

Fig. 8: Measured system efficiencies with gate drive loss included at V_{in} = 48 V.

TABLE II: Performance comparison of MLB-PoL converters using the inductors in this work and discrete inductors

	Efficiency including gate drive loss at V_{in} = 48 V			Power density @ V_{out} = 1.8 V & Dimensions
	V_{out} = 1 V	V_{out} = 1.2 V	V_{out} = 1.8 V	
Coupled L (This work)	**Peak: 91.5% Full load: 88.4%**	**Peak: 92.5% Full load: 89.4%**	**Peak: 94.4% Full load: 91.5%**	**474 W/in^3 26×18.4×7.8 mm**
Uncoupled L (This work)	Peak: 91.8% Full load: 87.9%	Peak: 92.8% Full load: 89.1%	Peak: 94.5% Full load: 91.6%	391 W/in^3 31.5×18.4×7.8 mm
Discrete L from [8]	Peak: 91.5% Full load: 87.2%	Peak: 92.4% Full load: 88.5%	Peak: 94.0% Full load: 91.3%	329 W/in^3 29×18.4×10.1 mm

Table II compares the efficiency and power density of the MLB-POL converters using the coupled/uncoupled integrated inductors presented in this work and the original discrete inductors (Pulse PG0702.601NL) used in [8]. All other components except the output inductors remain unchanged. The coupled inductors achieve 0.4% higher peak efficiency and 44% higher power density at V_{out} = 1.8 V compared to the discrete inductors.

IV. Conclusions

This work proposes a methodology to analyze the core size of ferrite gapped coupled inductors by using the magnetic flux model. A 55% core size reduction at D = 0.3 and K = -0.75 is predicted by the model and verified by experiment. By using the proposed coupled inductors in a 48-to-1.8 V MLB-PoL converter, the peak system efficiency reaches 94.4%, and the power density reaches 474 W/in^3. This converter benefits from a significant core size reduction due to strong magnetic coupling and high duty ratio. Both the efficiency and power density of this converter are higher than the existing MLB-PoL converter with discrete inductors.

V. Acknowledgment

The information, data, or work presented herein was funded in part by the Advanced Research Projects Agency-Energy (ARPA-E), U.S. Department of Energy, under Award Number DE-AR0000906 in the CIRCUITS program monitored by Dr. Isik Kizilyalli. The views and opinions of authors expressed herein do not necessarily state or reflect those of the United States Government or any agency thereof.

Rose Abramson was supported by the Department of Defense (DoD) through the National Defense Science & Engineering Graduate (NDSEG) Fellowship Program.

References

[1] J. Li, C. Sullivan, and A. Schultz, "Coupled-inductor design optimization for fast-response low-voltage dc-dc converters," in *APEC. Seventeenth Annual IEEE Applied Power Electronics Conference and Exposition (Cat. No.02CH37335)*, vol. 2, 2002, pp. 817–823 vol.2.

[2] P.-L. Wong, P. Xu, P. Yang, and F. Lee, "Performance improvements of interleaving vrms with coupling inductors," *IEEE Transactions on Power Electronics*, vol. 16, no. 4, pp. 499–507, 2001.

[3] Y. Yugang, Y. Dong, and F. C. Lee, "A new coupled inductors design in 2-phase interleaving vrm," in *2009 IEEE 6th International Power Electronics and Motion Control Conference*, 2009, pp. 344–350.

[4] A. Ikriannikov and T. Schmid, "Magnetically coupled buck converters," in *2013 IEEE Energy Conversion Congress and Exposition*, 2013, pp. 4948–4954.

[5] M. G. Chen and C. R. Sullivan, "Unified models for coupled inductors applied to multiphase pwm converters," *IEEE Transactions on Power Electronics*, pp. 1–1, 2021.

[6] P. S. Shenoy, M. Amaro, J. Morroni, and D. Freeman, "Comparison of a buck converter and a series capacitor buck converter for high-frequency, high-conversion-ratio voltage regulators," *IEEE Transactions on Power Electronics*, vol. 31, no. 10, pp. 7006–7015, 2016.

[7] J. Baek, P. Wang, S. Jiang, and M. Chen, "Lego-pol: A 93.1% 54v-1.5v 300a merged-two-stage hybrid converter with a linear extendable group operated point-of-load (lego-pol) architecture," in *2019 20th Workshop on Control and Modeling for Power Electronics (COMPEL)*, 2019, pp. 1–8.

[8] Z. Ye, R. A. Abramson, Y.-L. Syu, and R. C. N. Pilawa-Podgurski, "Mlb-pol: A high performance hybrid converter for direct 48 v to point-of-load applications," in *2020 IEEE 21st Workshop on Control and Modeling for Power Electronics (COMPEL)*, 2020, pp. 1–8.

[9] R. C. N. Pilawa-Podgurski, D. M. Giuliano, and D. J. Perreault, "Merged two-stage power converter architecture with soft charging switched-capacitor energy transfer," in *2008 IEEE Power Electronics Specialists Conference*, June 2008, pp. 4008–4015.

[10] R. C. N. Pilawa-Podgurski and D. J. Perreault, "Merged two-stage power converter with soft charging switched-capacitor stage in 180 nm cmos," *IEEE Journal of Solid-State Circuits*, vol. 47, no. 7, pp. 1557–1567, July 2012.

[11] W. G. Hurley and W. H. Wolfle, *Transformers and Inductors for Power Electronics - Theory, Design, and Applications*. Wiley, 2013.

[12] Texas Instruments, *Basic Calculation of a Buck Converter's Power Stage*, 2015. [Online]. Available: https://www.ti.com/lit/an/slva477b/slva477b.pdf

[13] Y. Jang, M. Jovanovic, and Y. Panov, "Multiphase buck converters with extended duty cycle," in *2006 IEEE Applied Power Electronics Conference and Exposition*, 2006, pp. 38–44.

[14] T. Ge, Z. Miao, and L. Liu, "Active cross-commutated (acc) buck converter," *IEEE Transactions on Industrial Electronics*, pp. 1–1, 2021.

[15] Z. Ye, Y. Lei, and R. C. N. Pilawa-Podgurski, "The cascaded resonant converter: A hybrid switched-capacitor topology with high power density and efficiency," *IEEE Transactions on Power Electronics*, vol. 35, no. 5, pp. 4946–4958, 2020.

[16] T. Ge, Z. Ye, R. Abramson, and R. C. N. Pilawa-Podgurski, "A 48-to-12 v cascaded resonant switched-capacitor converter achieving 4068 w/in^3 power density and 99.0% peak efficiency," in *2021 IEEE Applied Power Electronics Conference and Exposition (APEC)*, 2021.